Int. J. Electrochem. Sci., 15 **(2020)** 7152 – 7162, doi: 10.20964/2020.08.49

International Journal of ELECTROCHEMICAL SCIENCE
www.electrochemsci.org

Short Communication

Numerical Study on the Water Transport Through the Membrane of Proton Exchange Membrane Fuel Cells

Shian Li, Rongqiang Wei, Qiuwan Shen[*]*, Guogang Yang*[*]

Marine Engineering College, Dalian Maritime University, China.
[*]E-mail: shenqiuwan@dlmu.edu.cn and yanggg@dlmu.edu.cn

Received: 8 April 2020 / *Accepted:* 24 May 2020 / *Published:* 10 July 2020

A two-dimensional mathematical model is developed to study the water transport through the membrane. The transport processes include the electro-osmotic drag process and back diffusion process. And a non-equilibrium water sorption model is employed to describe the water absorption process in the catalyst layers. The effect of absorption coefficient of water on transport characteristics are comprehensively investigated. It is concluded that the cell performance and transport phenomena inside fuel cells are significantly affected by the water absorption process. The obtained polarization curves are presented and compared. The distributions of temperature, liquid water saturation, water content and local current density at cell voltages 0.6 V and 0.3V are also comprehensively analyzed.

Keywords: Proton exchange membrane fuel cells, Absorption process, Cell performance, Transport characteristics

1. INTRODUCTION

Proton exchange membrane fuel cells (PEMFCs) can be used as power supply for different applications [1-2]. In order to facilitate the commercialization of PEMFCs, the cell performance must be improved and the cost must be reduced. Therefore, experimental and numerical studies have already been performed to accelerate the process [3-8].

During the operating process of PEMFCs, the consumption of hydrogen/oxygen and the generation of water take place in the corresponding catalyst layers (CLs). Meanwhile, water is transported through the membrane. The transport processes include the electro-osmotic drag occurring from the anode CL to cathode CL and back diffusion occurring from the cathode CL to anode CL [9]. The protonic conductivity is associated with the water content of membrane [10]. A higher level water content leads to a higher protonic conductivity which decreases the proton transport resistance and the ohmic loss. The water transport process through the membrane strongly affects the cell performance.

Due to the relatively small size of fuel cells, computational fluid dynamics is extensively applied to examine the fundamental phenomena inside fuel cells. A one-dimensional, isothermal, and single-phase model was used to investigate the water transport mechanism through the membrane and its effects on cell performance [9]. A two-dimensional, non-isothermal, and single-phase model was adopted to investigate the effects of the porosity, the inlet velocity and the temperature on cell performance [11]. A three-dimensional, multiphase mixture model was employed to capture the liquid water transport behavior in the porous regions [12]. Non-equilibrium water sorption model has already been widely used to describe the water absorption process in CLs. It is assumed that water sorption process only takes place between vapor-dissolved phases and liquid-dissolved phases at anode CL and cathode CL, respectively. Meanwhile, different absorption coefficients of water were used in numerical models [13-18].

In this work, the process of water transport through the membrane was modeled and the water sorption process takes place between vapor-dissolved and liquid-dissolved phases at CLs. In addition, the effect of absorption coefficient of water on cell performance and transport phenomena are comprehensively investigated. The corresponding polarization curves and distributions of temperature, liquid water saturation, water content and current density are comprehensively analyzed.

2. MATHEMATICAL MODEL DESCRIPTION

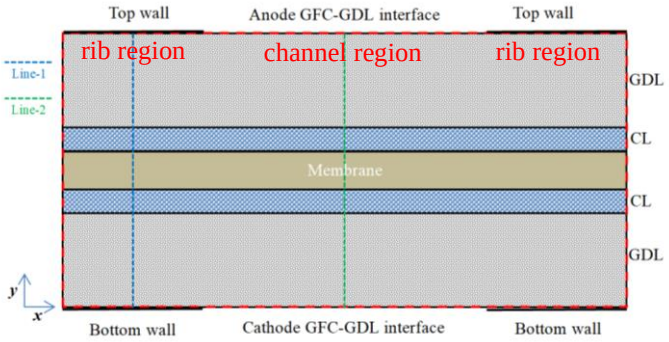

Figure 1. Computational domain of the present study.

Table 1. Geometric parameters of the physical model.

Parameter	Value	Unit
Cell width	2	mm
GFC width	1	mm
GDL thickness	0.2	mm
CL thickness	0.01	mm
Membrane thickness	0.05	mm

The computational domain of this study is presented in Figure 1. It consists of the GDL, CL and membrane. The geometric parameters are summarized in Table 1. Line-1 and Line-2 represent the

middle position of wall and fuel cell. The operating pressure and temperature of fuel cell is 1.0 atm and 353 K, respectively. The fluid flow is laminar flow. Ideal gas law is used. The GDLs and CLs are homogeneous and isotropic. The generated water is in dissolved phase [3-4].

2.1 Governing equations

The governing equations and parameters used in this study are presented in Table 2 and Table 3, respectively. The process of water transport through the membrane is described by the dissolved water transport equation. And the water sorption process takes place between vapor-dissolved and liquid-dissolved phases at anode and cathode CLs. In the descriptions of source terms, S_{vd} represents the water sorption process between the vapor phase and dissolved phase. And S_{ld} represents the water sorption process between the liquid phase and dissolved phase. γ denotes the absorption coefficient of water. And the corresponding source terms of governing equations are summarized in Table 4.

Table 2. Governing equations of this study.

Species equation:	$0 = \nabla \cdot \left(\rho D_{eff,i} \nabla Y_i\right) + S_i$
Energy equation:	$0 = \nabla \cdot \left(k_{eff} \nabla \mathrm{T}\right) + S_T$
Charge equation:	$\nabla \cdot \left(\sigma_{eff,s} \nabla \phi_s\right) + S_s = 0$ $\nabla \cdot \left(\sigma_{eff,m} \nabla \phi_m\right) + S_m = 0$
Liquid water transport equation:	$0 = \nabla \cdot (\rho_l D_s \nabla s) + S_l$
Dissolved water transport equation:	$-\nabla \cdot \left(\frac{n_d}{F} \sigma_m \nabla \phi_m\right) = \nabla \cdot \left(\frac{\rho_m}{M_m} D_\lambda \nabla \lambda\right) + S_d$

Table 3. Parameters used in this study [3].

Parameter	Value	Units
Platinum loading, m_{pt}	0.4	mg cm^{-2}
Platinum density, ρ_{pt}	2.145×10^4	kg m^{-3}
Carbon loading, m_c	0.6	mg cm^{-2}
Carbon density, ρ_c	1.8×10^3	kg m^{-3}
Dry membrane density, ρ_m	1.98×10^3	kg m^{-3}
Membrane equivalent weight, M_m	1.1	kg mol^{-1}
Porosity of GDL, ε_{GDL}	0.6	-
Anode reference exchange current density, i_a^{ref}	100	A m^{-2}
Cathode reference exchange current density, i_c^{ref}	$10^{(0.03741*T-16.96)}$	A m^{-2}
Anode transfer coefficient, α_a	0.5	-
Cathode transfer coefficient, α_c	1	-
Reference hydrogen concentration, $c_{H_2}^{ref}$	56.4	mol m^{-3}
Reference oxygen concentration, $c_{O_2}^{ref}$	3.39	mol m^{-3}
Hydrogen Henry's constant, H_{H_2}	4.56×10^3	Pa m^3 mol^{-1}

Oxygen Henry's constant, H_{O_2}	$0.101325e^{(-666/T+14.1)}$	Pa m^3 mol^{-1}
Thermal conductivity of GDL/CL, $k_{GDL/CL}$	1.7/0.3	W m^{-1} K^{-1}
Thermal conductivity of membrane, k_m	0.25	W m^{-1} K^{-1}
Electrical conductivity of GDL/CL, $\sigma_{s,GDL/CL}$	5000/2000	S m^{-1}
Entropy of hydrogen oxidation, ΔS_a	0.104	J mol^{-1} K^{-1}
Entropy of oxygen reduction, ΔS_c	-326.36	J mol^{-1} K^{-1}
Latent heat of condensation/evaporation, Δh_{lg}	2.36×10^6	J kg^{-1}
Liquid water viscosity, μ_l	3.517×10^{-4}	Pa s
Surface tension, σ	0.0625	N m^{-1}
Contact angle of GDL/CL, $\theta_{GDL/CL}$	110°/95°	-
Condensation rate, γ_{con}	100	s^{-1}
Evaporation rate, γ_{evap}	100	s^{-1}
Permeability of GDL, K_{GDL}	5.6×10^{-12}	m^2
Permeability of CL, K_{CL}	1.0×10^{-13}	m^2
Binary diffusivity, $D_{H_2-H_2O}$	9.15×10^{-5}	m^2 s^{-1}
Binary diffusivity, $D_{O_2-H_2O}$	2.82×10^{-5}	m^2 s^{-1}
Binary diffusivity, $D_{O_2-N_2}$	2.2×10^{-5}	m^2 s^{-1}
Binary diffusivity, $D_{H_2O-N_2}$	2.56×10^{-5}	m^2 s^{-1}

2.2 Numerical implementation and boundary conditions

A two-dimensional model is developed by using the ANSYS FLUENT. And the user defined functions are also used for the implementation of the present model. The boundary conditions of the computational domain are as follows:

Anode GFC-GDL interface:

$$Y_{H_2} = Y_{H_{2,in}}, Y_{H_2O} = Y_{H_2O,in}, s = 0$$

Cathode GFC-GDL interface:

$$Y_{O_2} = Y_{O_{2,in}}, Y_{H_2O} = Y_{H_2O,in}, s = 0$$

Top walls:

$$\phi_s = 0, T = T_{cell}$$

Bottom walls:

$$\phi_s = V_{cell}, T = T_{cell}$$

Table 4. Source terms of the governing equations.

Descriptions	Units
$S_{H_2} = -\frac{j_a}{2F} M_{H_2}$ $Anode\ CL$	kg m^{-3} s^{-1}
$S_{O_2} = -\frac{j_c}{4F} M_{O_2}$ $Cathode\ CL$	kg m^{-3} s^{-1}
$S_{wv} = -S_l - S_{vd} M_{H_2O}$ $Anode\ and\ cathode\ CLs$	kg m^{-3} s^{-1}
$S_{wv} = -S_l$ $Anode\ and\ cathode\ GDLs$	

$S_T = j_a\eta_a - \frac{T\Delta S_a}{2F} j_a + \sigma_{eff,m}\|\nabla\phi_m\|^2 + \sigma_{eff,s}\|\nabla\phi_s\|^2 + (S_l - S_{ld})\Delta h_{lg}$ *Anode CL*	W m^{-3}
$S_T = j_c\eta_c - \frac{T\Delta S_c}{4F} j_c + \sigma_{eff,m}\|\nabla\phi_m\|^2 + \sigma_{eff,s}\|\nabla\phi_s\|^2 + (S_l - S_{ld})\Delta h_{lg}$ *Cathode CL*	
$S_T = \sigma_{eff,m}\|\nabla\phi_m\|^2$ *membrane*	
$S_T = \sigma_{eff,s}\|\nabla\phi_s\|^2 + S_l\Delta h_{lg}$ *Anode and cathode GDLs*	
$S_s = -j_a$ *Anode CL*	A m^{-3}
$S_s = +j_c$ *Cathode CL*	
$S_m = +j_a$ *Anode CL*	A m^{-3}
$S_m = -j_c$ *Cathode CL*	
$S_l = S_{phase} - S_{ld}$ *Anode and cathode GDLs and CLs*	kg m^{-3} s^{-1}
$S_{phase} = \begin{cases} \gamma_{cond}\frac{\varepsilon(1-s)}{RT} M_{H_2O}(P_{wv} - P_{sat}) & P_{wv} \geq P_{sat} \\ \gamma_{evap}\frac{\varepsilon s}{RT} M_{H_2O}(P_{wv} - P_{sat}) & P_{wv} < P_{sat} \end{cases}$	kg m^{-3} s^{-1}
$S_d = S_{vd} + S_{ld}$ *Anode CL*	mol m^{-3} s^{-1}
$S_d = S_{vd} + S_{ld} + S_\lambda$ *Cathode CL*	
$S_{vd} = (1-s)\gamma\frac{\rho_m}{M_m}(\lambda^{eq} - \lambda)$ *Anode and cathode CLs*	
$S_{ld} = s\gamma\frac{\rho_m}{M_m}(\lambda^{eq} - \lambda)$ *Anode and cathode CLs*	
$S_\lambda = \frac{j_c}{2F}$ *Cathode CL*	

3. RESULTS AND DISCUSSION

The water sorption process only takes place between vapor-dissolved phases or liquid-dissolved phases at CLs in the previous studies [13-18]. In this study, it is assumed that the water sorption process takes place between vapor-dissolved and liquid-dissolved phases at CLs. The effect of absorption coefficient of water on cell performance are presented in Fig.2. The coefficient of 1.0 is widely used in mathematical models. In this study, the corresponding absorption coefficients of water are 0.5, 1.0 and 1.5. The polarization curve is used to assess the cell performance. It is clearly seen that a higher current density is obtained when a lower coefficient value is used in the model. The current density is 1.30 A/cm^2 for the case at cell voltage 0.3 V with the coefficient value of 0.5, the corresponding current density is 1.26 A/cm^2 for the case with the coefficient value of 1.0, and the corresponding current density is 1.24 A/cm^2 for the case with the coefficient value of 1.5. It is concluded that the current density increases with decreasing absorption coefficient of water at low cell voltages. And the current density is not affected at high and medium cell voltages. In the following section, the distributions of temperature, liquid water saturation, water content and local current density at cell voltages 0.6 V and 0.3V are presented and analyzed.

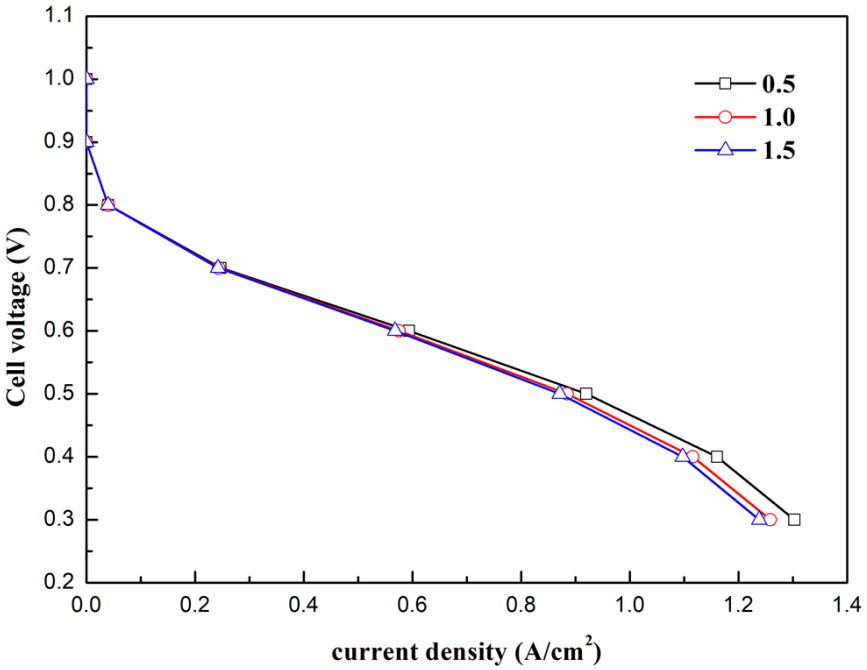

Figure 2. Effect of the absorption coefficient of water (γ=0.5, 1.0, 1.5) on the polarization curve.

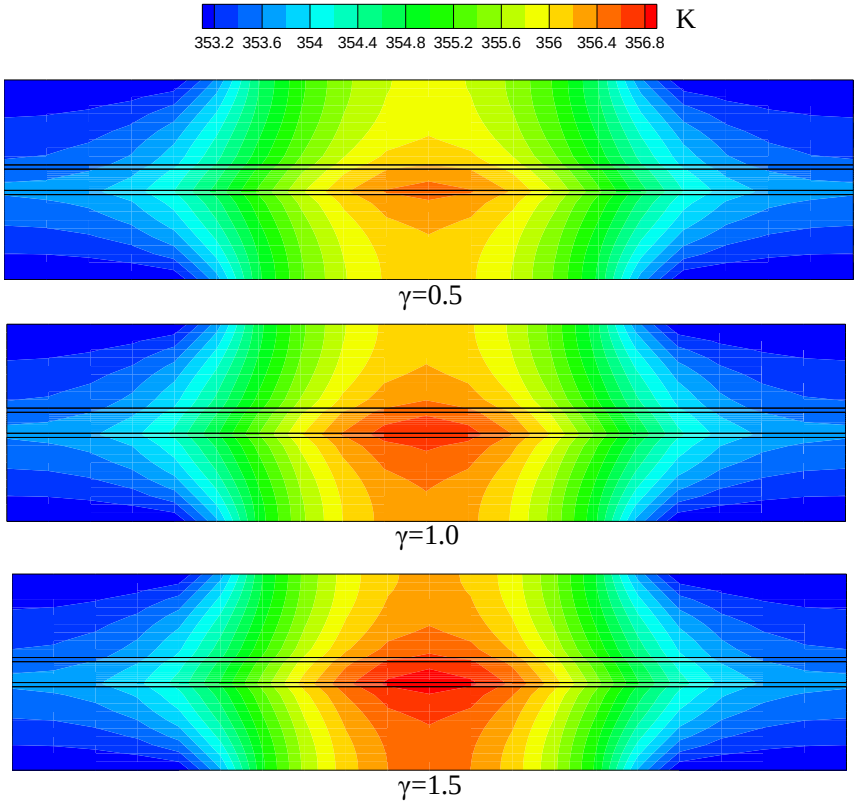

Figure 3. Effect of the absorption coefficient of water (γ=0.5, 1.0, 1.5) on temperature distribution of fuel cells at cell voltage 0.6 V.

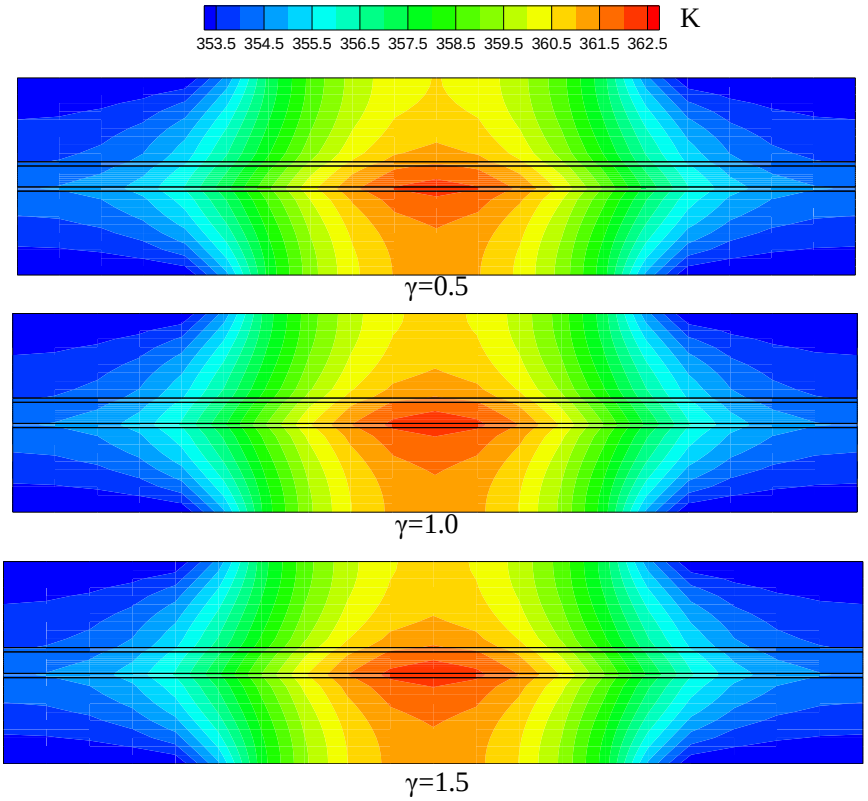

Figure 4. Effect of the absorption coefficient of water (γ=0.5, 1.0, 1.5) on temperature distribution of fuel cells at cell voltage 0.3 V.

The temperature distributions of fuel cells at 0.6 V and 0.3 V are shown in Figs. 3-4. It is clearly seen that the temperature distribution is slightly affected by the absorption coefficient of water. The membrane must be well hydrated to increase the protonic conductivity and then decrease the ohmic loss.

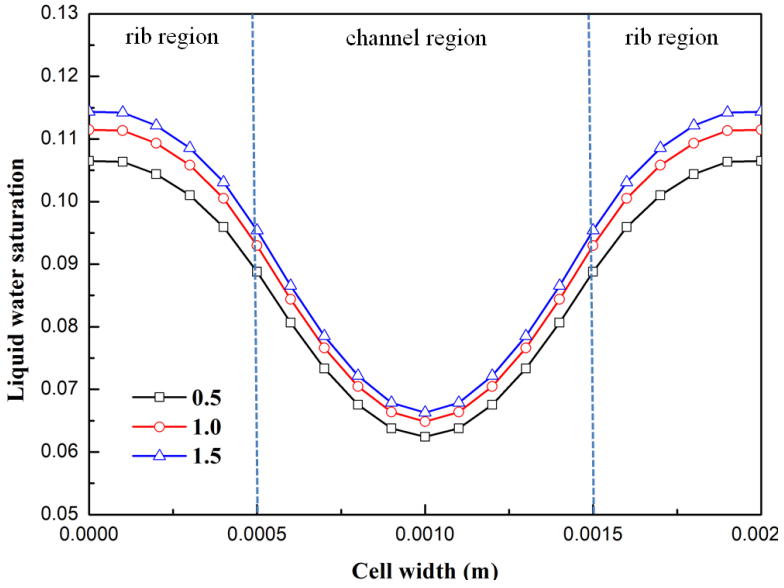

Figure 5. Effect of the absorption coefficient of water (γ=0.5, 1.0, 1.5) on liquid water saturation distribution at the cathode GDL-CL interface of fuel cells at cell voltage 0.6 V.

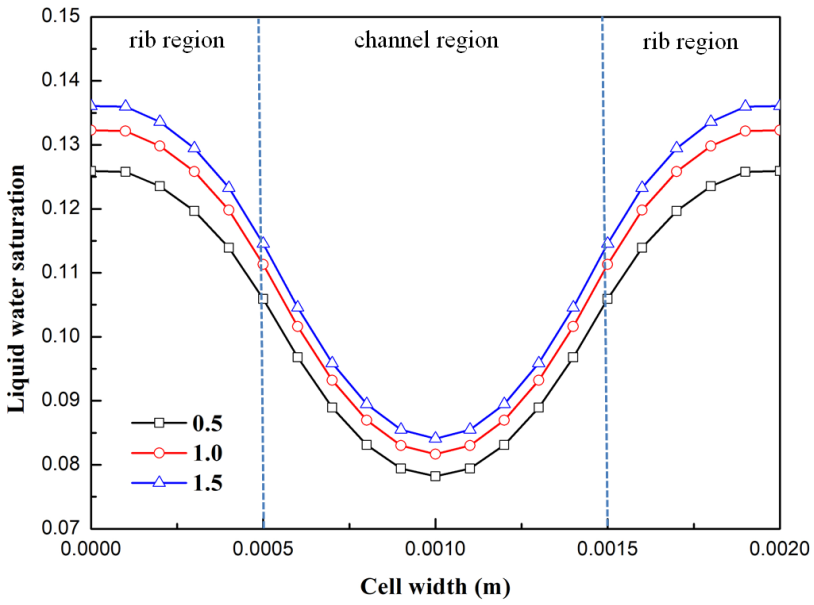

Figure 6. Effect of the absorption coefficient of water (γ=0.5, 1.0, 1.5) on liquid water saturation distribution at the cathode GDL-CL interface of fuel cells at cell voltage 0.3 V.

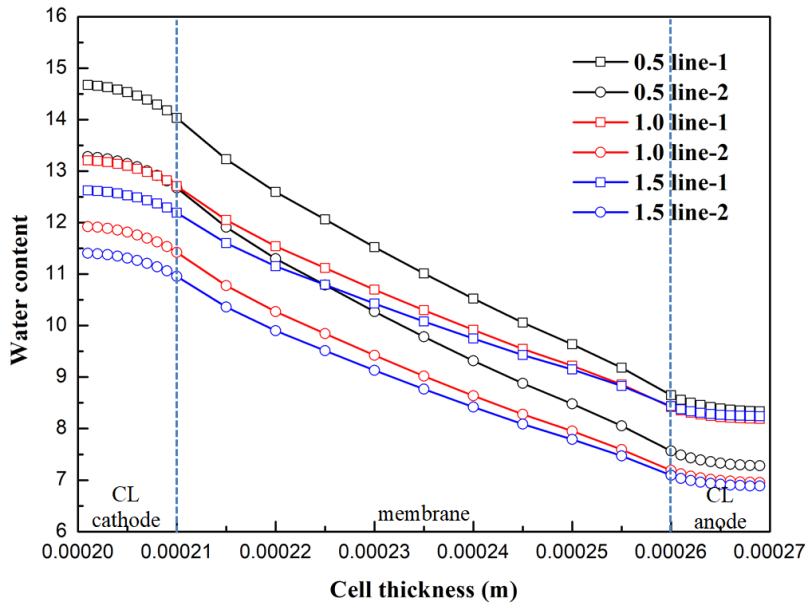

Figure 7. Effect of the absorption coefficient of water (γ=0.5, 1.0, 1.5) on water content distribution of fuel cells at cell voltage 0.6 V.

However, the liquid water can also block the gas transport electrochemical reaction processes. The liquid water saturation variations at the cathode GDL-CL interface at cell voltages 0.6 V and 0.3 V are shown in Figs. 5-6. It can be seen that the distribution profile is not affected by the absorption coefficient of water, but the liquid water saturation level is significantly influenced. It can be observed that the liquid water saturation increases with increasing absorption coefficient of water. In addition, the

liquid water saturation level is increased when the cell voltage varies from 0.6 V to 0.3 V. This can be explained by the source term of S_{ld}, which is proportional to the absorption coefficient of water.

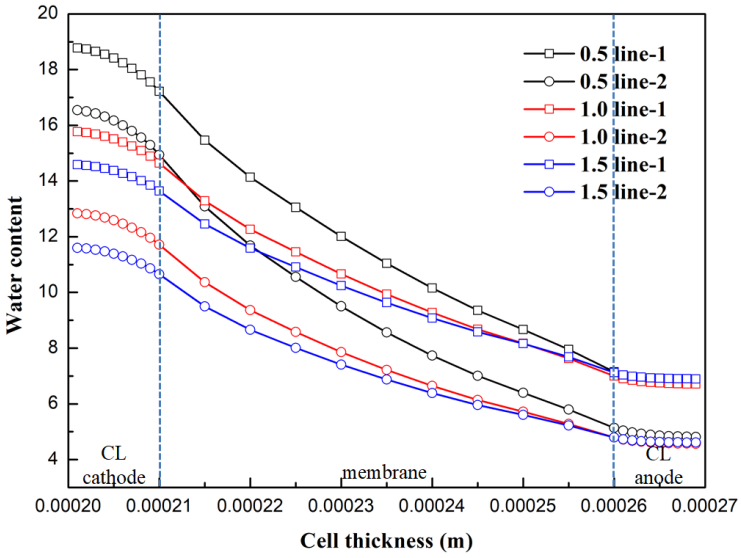

Figure 8. Effect of the absorption coefficient of water (γ=0.5, 1.0, 1.5) on water content distribution of fuel cells at cell voltage 0.3 V.

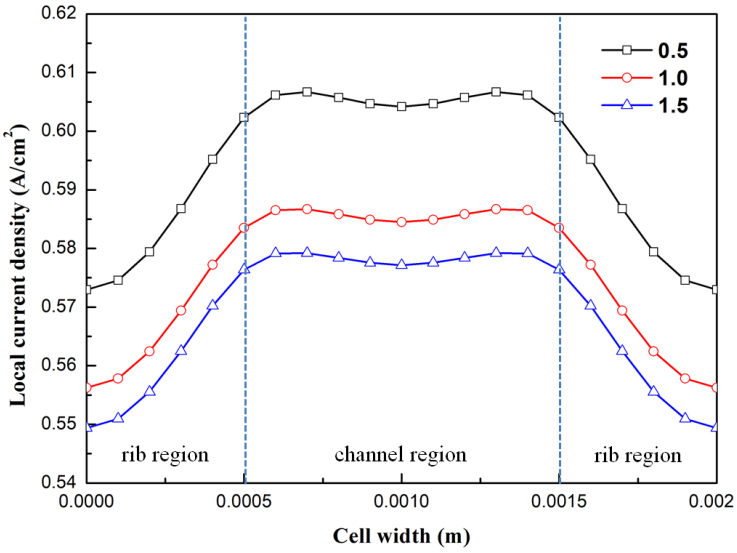

Figure 9. Effect of the absorption coefficient of water (γ=0.5, 1.0, 1.5) on local current density distribution of fuel cells at cell voltage 0.6 V.

The protonic conductivity is a function of water content and protonic conductivity increases with increasing water content. The water content at the line-1 and line-2 at cell voltages 0.6 V and 0.3 V are presented in Figs. 7-8. It is observed that water content decreases from cathode to anode and water content at line-2 is lower than that at line-1. Similar distributions of water content were also reported by other researchers [10, 16]. This is mainly attributed to the liquid water saturation. And the water content

decreases with increasing absorption coefficient of water, especially at the cathode CL and membrane regions. This indicates that a higher coefficient in the non-equilibrium water sorption model can lead to a small variation of water content through the membrane. In addition, the water content variation from the anode to the cathode increases when the cell voltage changes from 0.6 V to 0.3 V. These are determined by the combined effect of electro-osmotic drag and back diffusion processes.

The local current densities at cell voltages 0.6 V and 0.3 V are shown in Figs. 9-10. It is clear that current density at the channel region is larger than that at the rib regions. The current density increases with the decreasing absorption coefficient of water. This is consistent with the current density reported in Fig. 2. The profile of current density at the channel region changes when the cell voltage varies from 0.6 V to 0.3 V. The trend of current density distribution at the cell voltage 0.6 V is not affected by the absorption coefficient of water, while it is slightly changed at the cell voltage 0.3 V with different absorption coefficients of water.

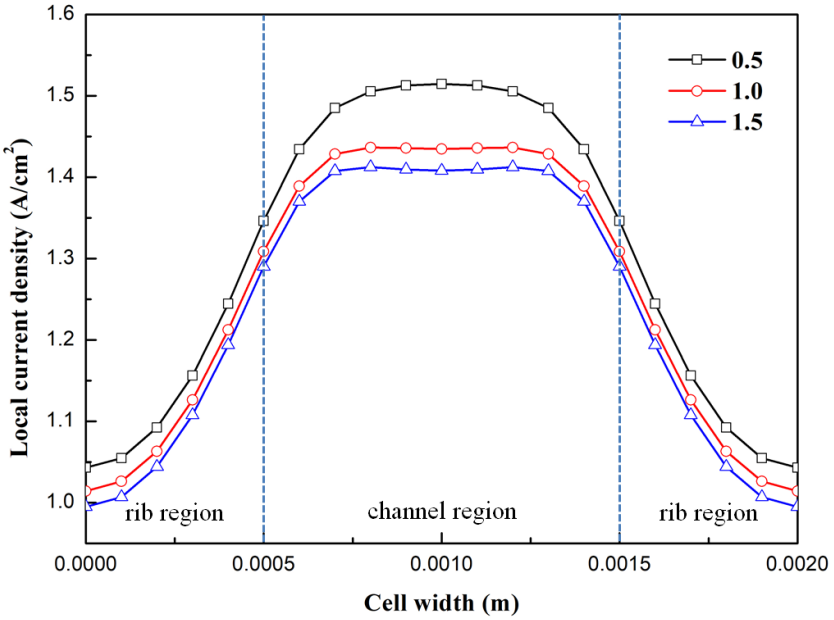

Figure 10. Effect of the absorption coefficient of water (γ=0.5, 1.0, 1.5) on local current density distribution of fuel cells at cell voltage 0.3 V.

4. CONCLUSIONS

The effect of absorption coefficient of water on cell performance and transport characteristics are comprehensively investigated by using a two-dimensional model including the processes of water transport through the membrane and water sorption. The current density increases with decreasing absorption coefficient of water at low cell voltages. And the current density is not affected at high and medium cell voltages. The liquid water saturation increases with increasing absorption coefficient of water. The water content decreases with increasing absorption coefficient of water, especially at the cathode CL and membrane regions. In addition, the local current density is also affected by the

absorption coefficient of water. The obtained results provide and improve the understanding of the processes of water transport through the membrane and water sorption.

ACKNOWLEDGMENTS
The authors gratefully acknowledge the financial supports from National Natural Science Foundation of China (No.51779025). This work is also funded by the Fundamental Research Funds for the Central Universities of China (No. 3132019327), China Postdoctoral Science Foundation (No.2019M651097 and No.2019M651094) and Natural Science Foundation of Liaoning Province (No.2019-BS-026 and No.2019-ZD-0154).

References

1. T.D. Tran, S. Huang, D.H. Vu, V.N. Duy, *Int. J. Electrochem. Sci.,* 13 (2018) 10480.
2. B. Lee, K. Park, H.M. Kim, *Int. J. Electrochem. Sci.,* 8 (2013) 219.
3. S.A. Li, R.Q. Wei, Y.X. Qi, G.G. Yang, Q.W. Shen, *Int. J. Electrochem. Sci.,* 14 (2019) 11367.
4. S.A. Li, R.Q. Wei, G.L. Zhang, Y.X. Qi, G.G. Yang, Q.W. Shen, *Int. J. Electrochem. Sci.,* 15 (2020) 4138.
5. M. Arif, S.C.P. Cheung, J. Andrews, Int. J. Hydrogen Energy, 45 (2020) 2206.
6. Z. Penga, C. Bergbreiter, F. Barbir, J. Scholta, *Energy Convers. Manag*., 189 (2019) 167.
7. S.A. Li, B. Sunden, *Int. J. Hydrogen Energy,* 43 (2018) 16279.
8. E.E. Kahveci, I. Taymaz, *Fuel*, 253 (2019) 1274.
9. T.E. Springer, T.A. Zawodzinski, S. Gottesfeld, *J. Electrochem. Soc.*, 138 (1991) 2334.
10. S.A. Li, J.L. Yuan, M. Andersson, G.N. Xie, B. Sunden, *Int. J. Energy Res.*, 41 (2017) 2034.
11. V. Gurau, H.T. Liu, S. Kakac, *AICHE J.*, 44 (1998) 2410.
12. H. Meng, C.Y. Wang, *J. Electrochem. Soc.*, 152 (2005) A1733.
13. S.A. Li, J.L. Yuan, M. Andersson, G.N. Xie, B. Sunden, *J. Electrochem. Energy Convers. Storage*, 14 (2017) 031007.
14. S.A. Li, J.L. Yuan, G.N. Xie, B. Sunden, *Int. J. Hydrogen Energy,* 43 (2018) 8451.
15. X.G. Yang, Q. Ye, P. Cheng, *Int. J. Hydrogen Energy*, 36 (2011) 12524.
16. H. Wu, P. Berg, X.G. Li, *Appl. Energy*, 87 (2010) 2778.
17. H. Wu, X. Li, P. Berg, *Electrochim. Acta*, 54 (2009) 6913.
18. P. Havaej, *Energy*, 182 (2019) 656.